Supplemental Information

Charge target collection from different triboelectrification domains by electrostatic induction and polarization enabled air discharges

Kaixian Li‡[a], Siqi Gong‡[a], Shaoke Fu‡[a], Hengyu Guo[a], Chuncai Shan[a], Huiyuan Wu[a], Jian Wang[a], Shuyan Xu[a], Gui Li[a], Qionghua Zhao[a], Xue Wang[a]* and Chenguo Hu[a]*

[a] School of Physics, Chongqing Key Laboratory of Interface Physics in Energy Conversion, Chongqing University, Chongqing, 400044, P. R. China.

‡These authors contributed equally to this work.

*Correspondence: xuewang@cqu.edu.cn (X. Wang); hucg@cqu.edu.cn (C. Hu)

Content
Supplementary Figures:

Supplementary Notes:

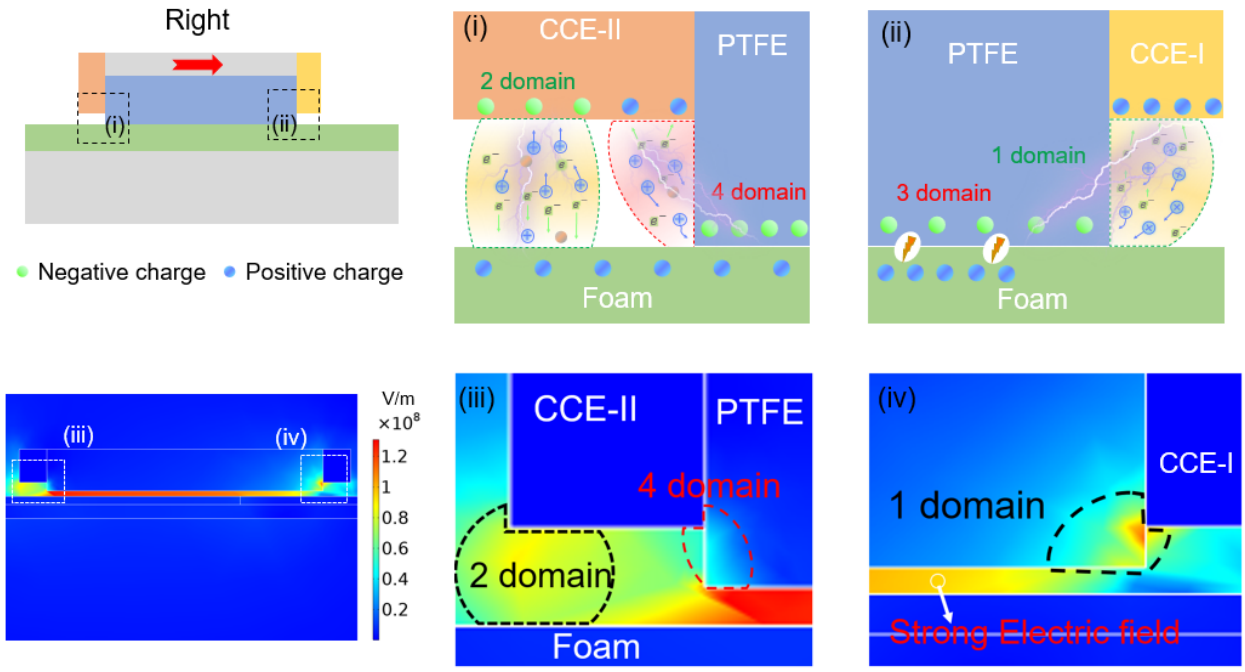

Figure S1. Four domains' discharge paths and corresponding electric field distribution of conventional DC-TENG.

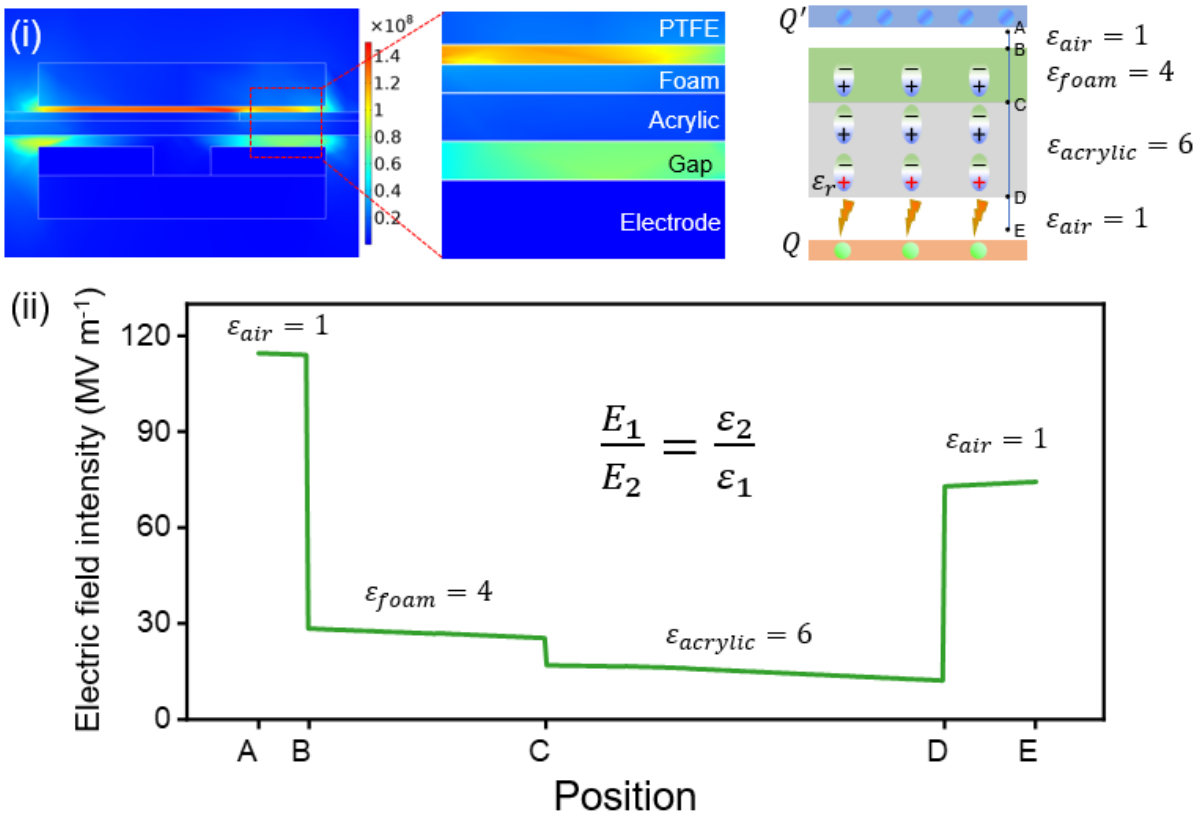

Figure S2. Simulated electric field intensity inside the materials during the DPD process.

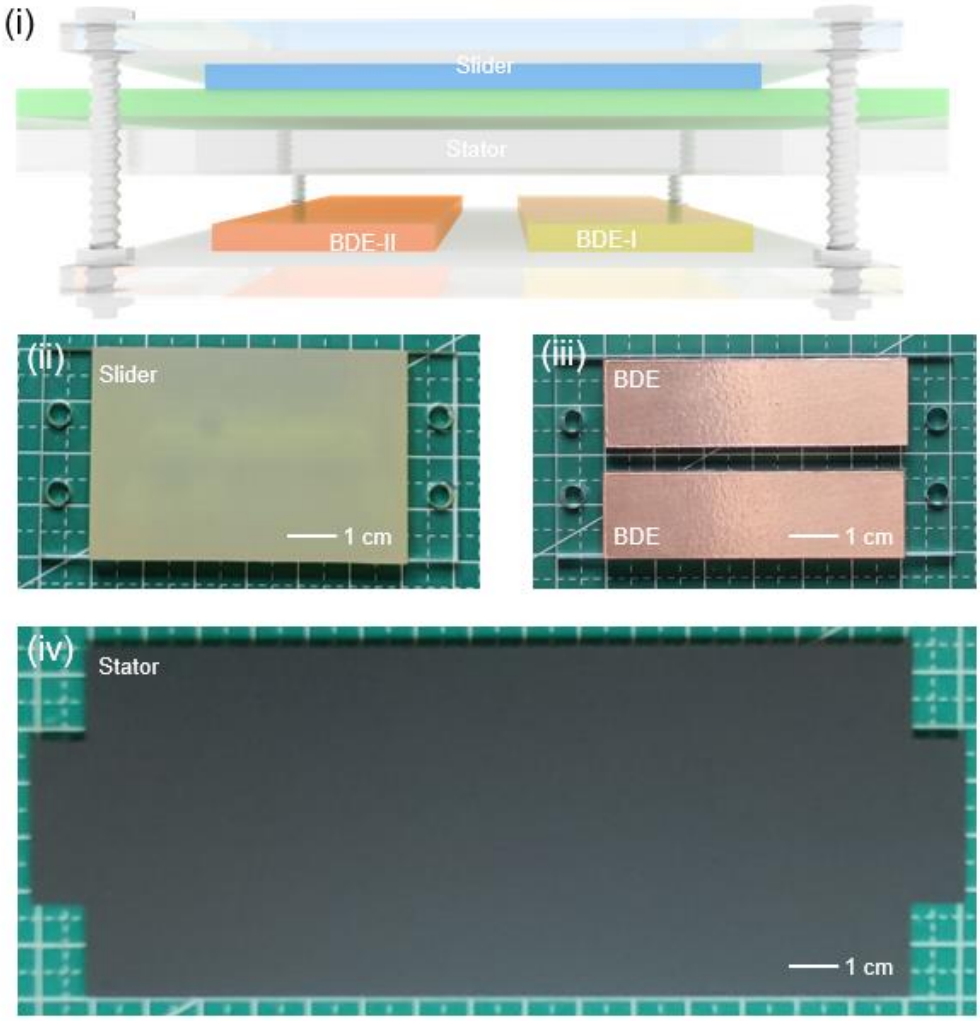

Figure S3. Schematic diagram of the structure of CTC-TENG. (i) 3D structure diagram. Digital photograph of (ii) the slider, (iii) the BDEs and (iv) the stator.

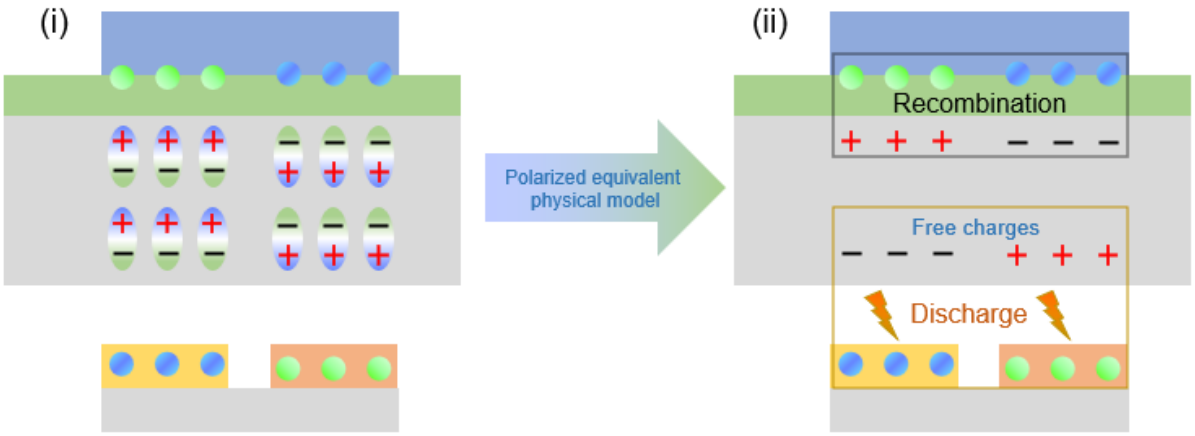

Figure S4. Equivalent charge physical model in dielectric polarization enabled discharges.

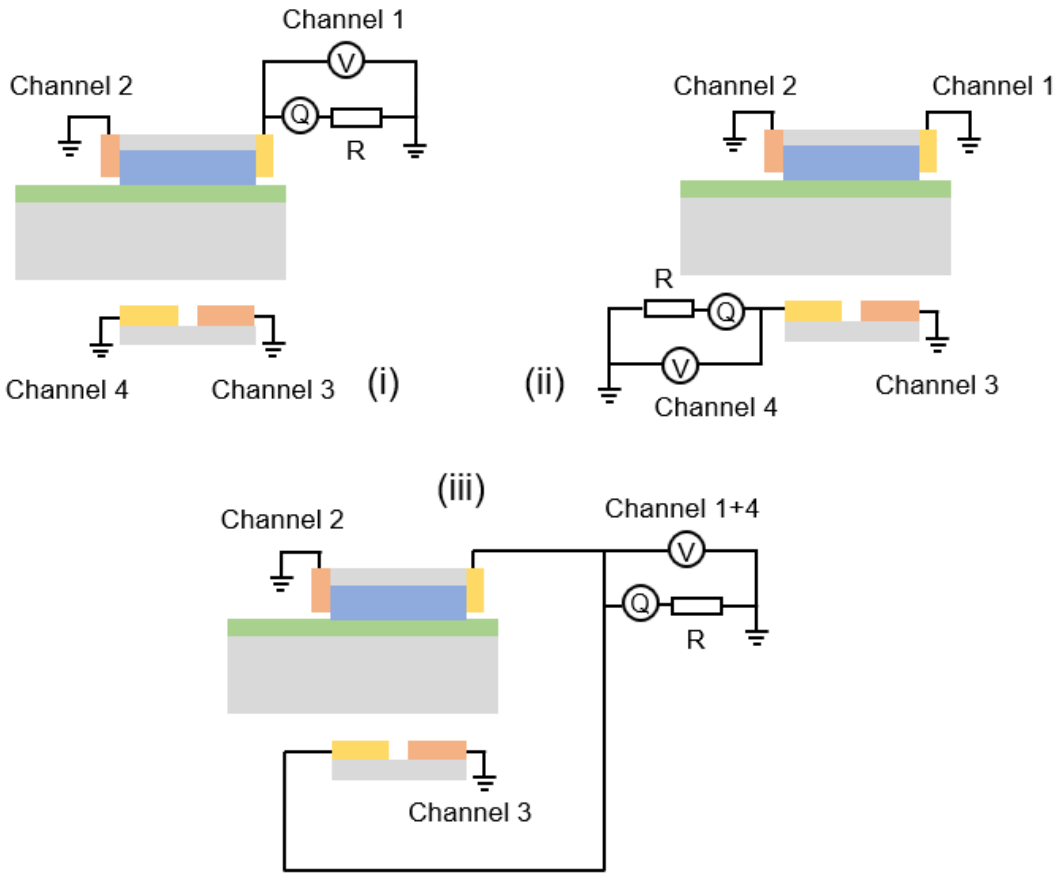

Figure S5. Circuit connection ways for measuring voltage-charge curve. (i) individual measure channel 1. (ii) individual measure channel 4. (iii) channel 1 and channel 4 are connected in parallel as a unified channel.

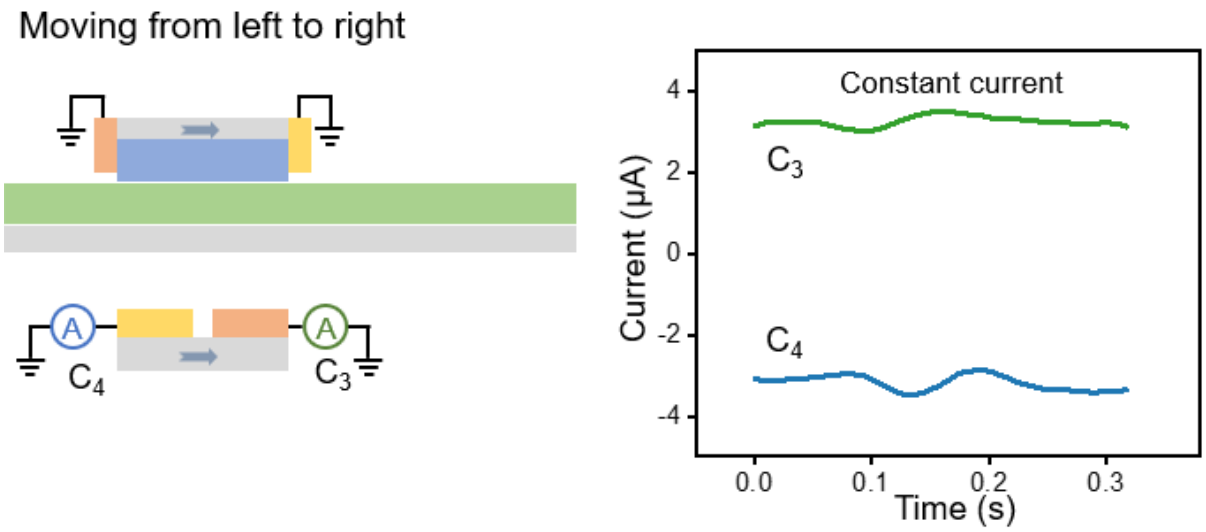

Figure S6. Output current curves of channel 3 and channel 4 when the slider and BDEs move synchronously from left to right.

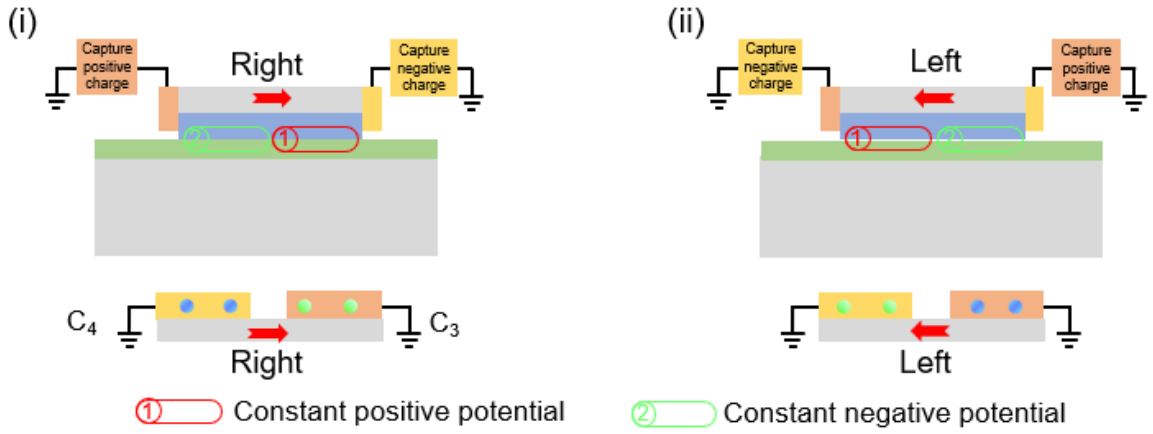

Figure S7. Equivalent potential of the tribo-layer interface at different sliding directions. (i) slider and BDEs move synchronously from left to right. (ii) slider and BDEs move synchronously from right to left.

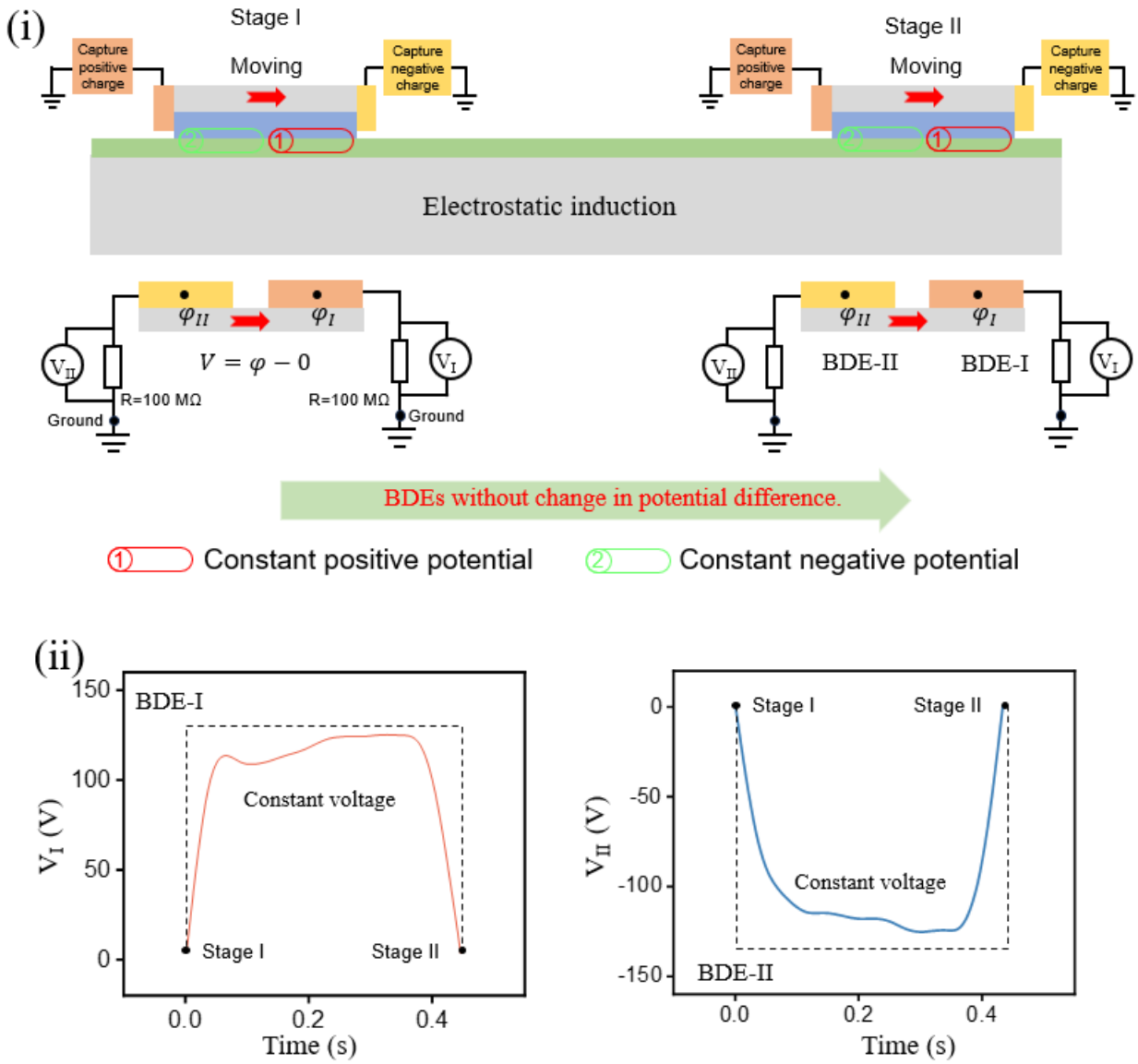

Figure S8. Non-electrostatic induction in dielectric polarization enabled discharges. (i) From stage I to stage II, BDEs without change in potential difference. (ii) The potential curve of BDE-I and BDE-II from stage I to stage II.

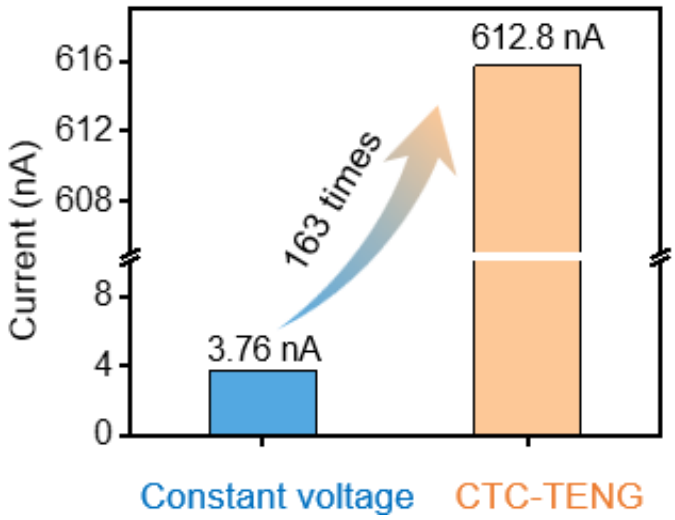

Figure S9. Comparison of the current values between constant voltage (applied voltage at 8 kV) and CTC-TENG.

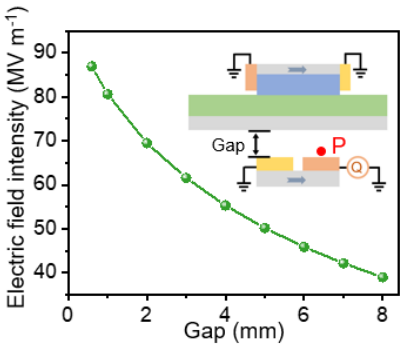

Name	Parameters for simulation
Air	Permittivity: 1
PTFE	Thickness: 1.5 mm Permittivity: 3 Surface charge density: -1.2 mC m^{-2}
Foam	Thickness: 0.3 mm Permittivity: 4 Surface charge density: 1.2 mC m^{-2}
Cu	Permittivity: 999999

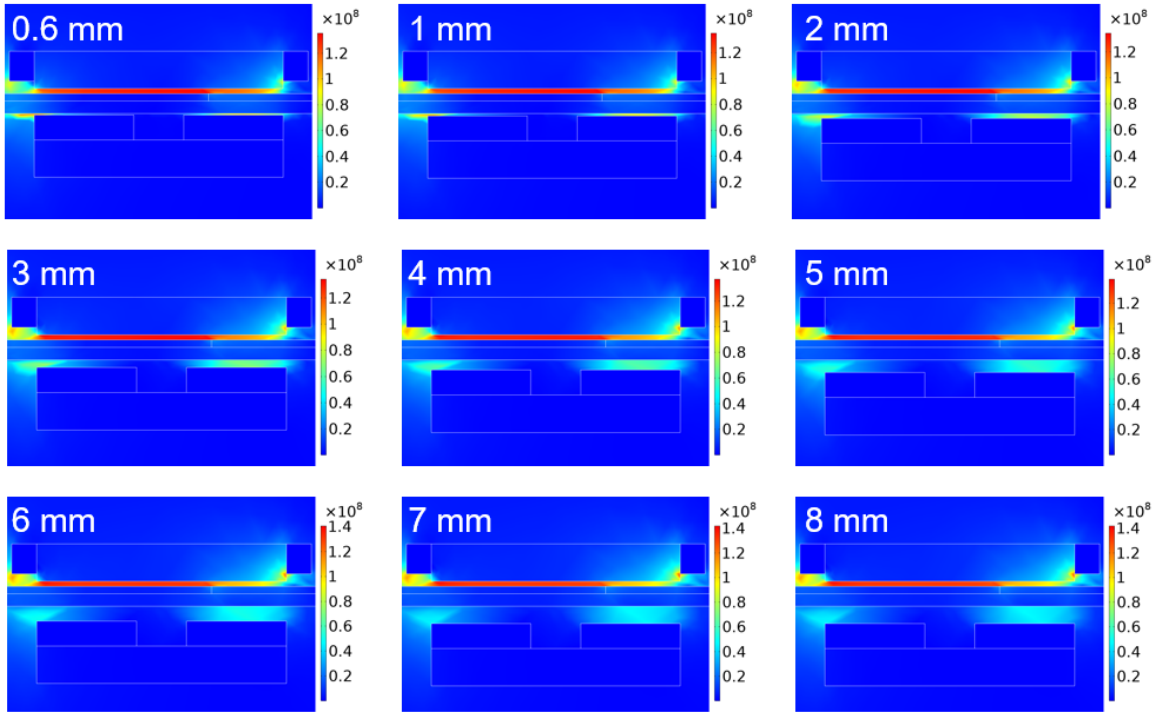

Figure S10. Electric field intensity at the P point is simulated when the gap between substrate and BDEs changes.

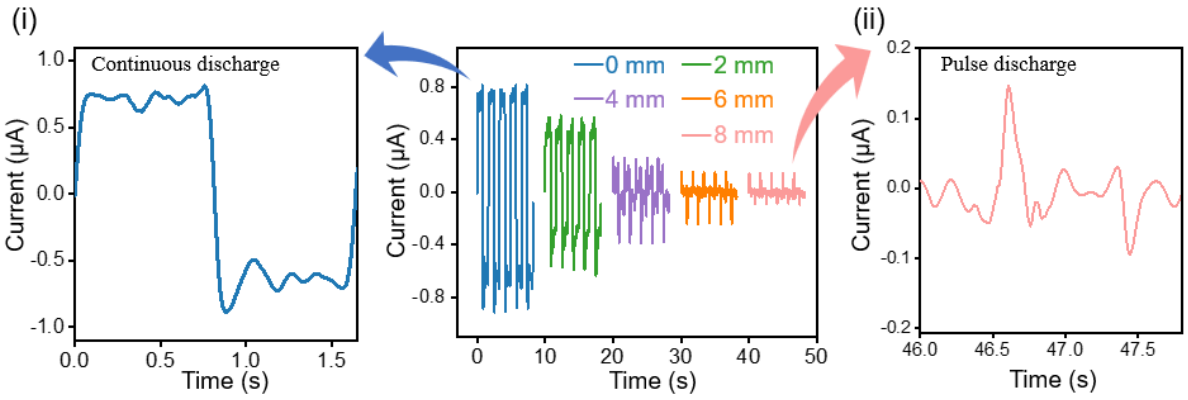

Figure S11. Output current of the CTC-TENG with different air gaps between BDEs and substrate. (i) continuous discharge. (ii) pulse discharge.

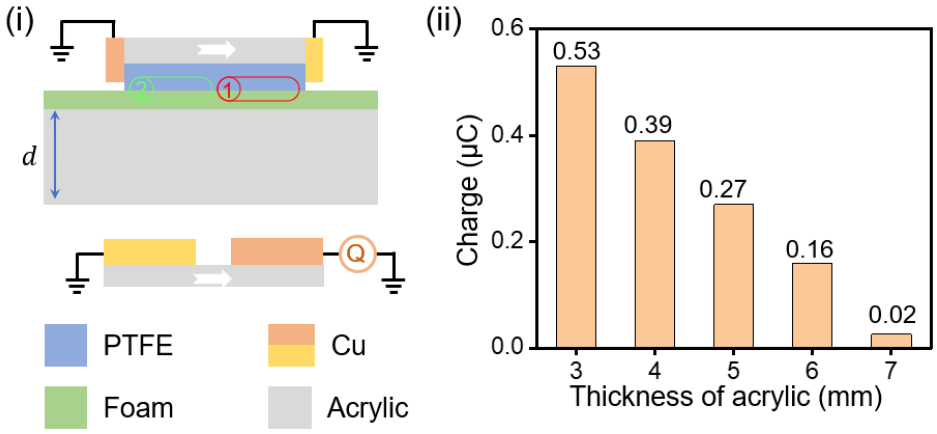

Figure S12. Output charge of the BDE with different thicknesses of acrylic substrate.

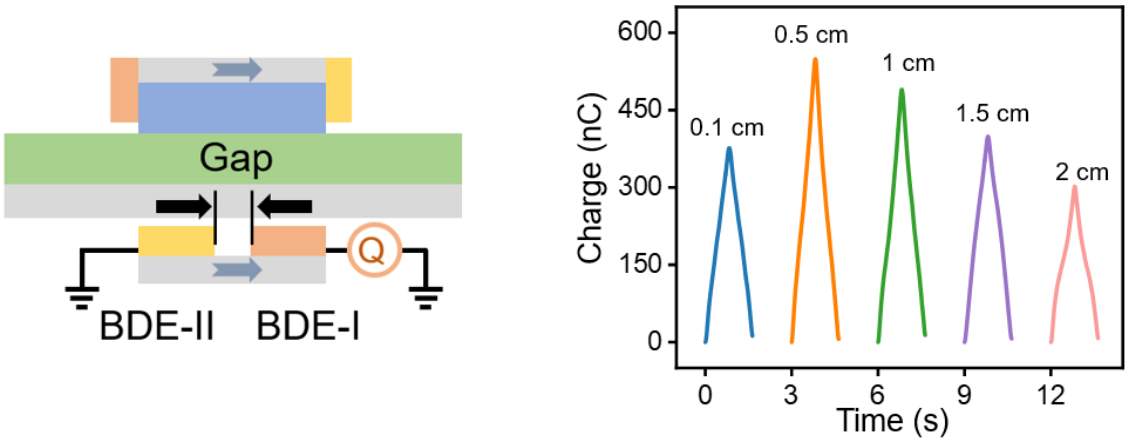

Figure S13. Output charge of the bottom dynamic electrode with different gaps.

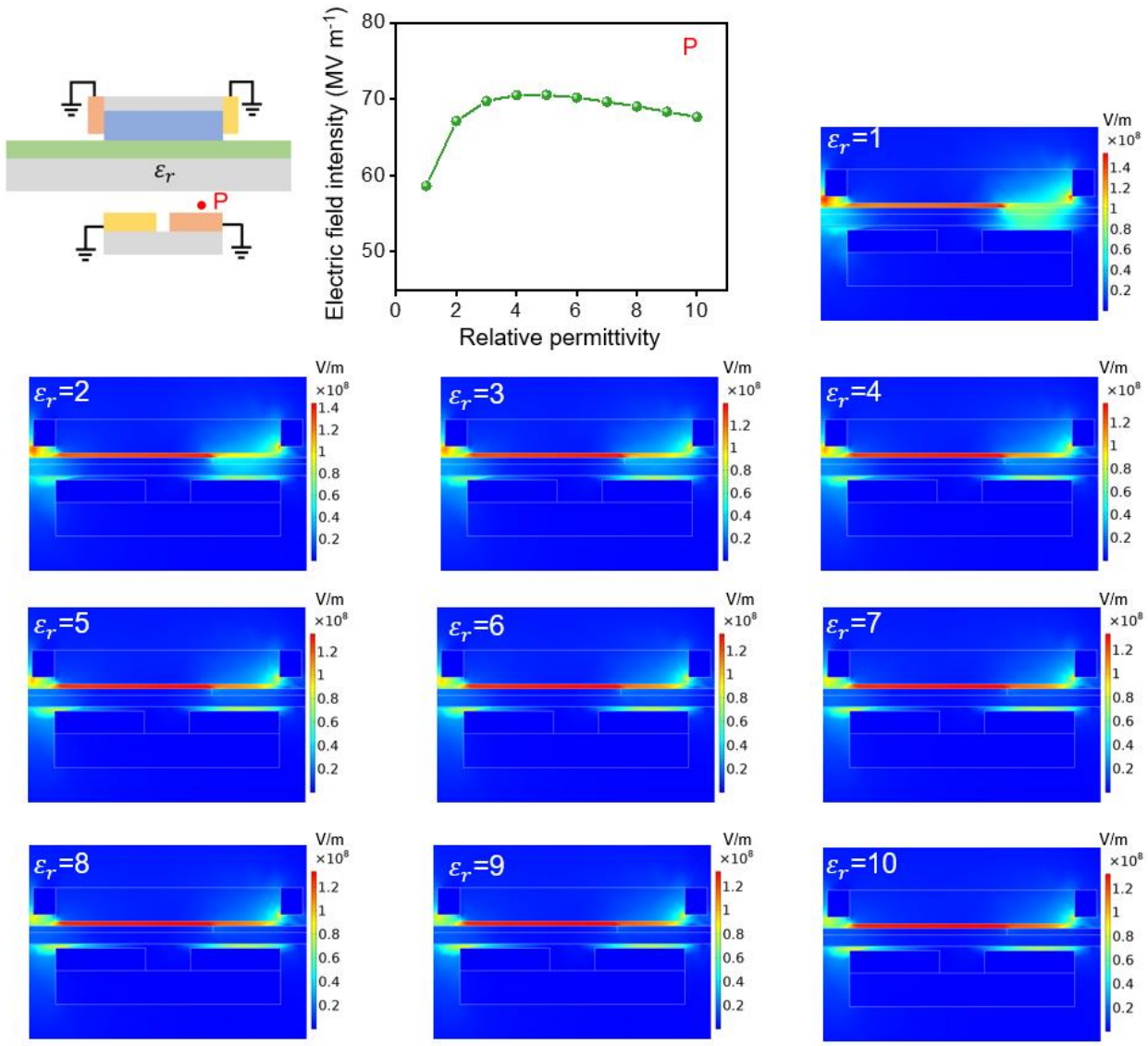

Figure S14. Simulated electric field intensity between BDEs and substrate with different relative permittivity of the substrate.

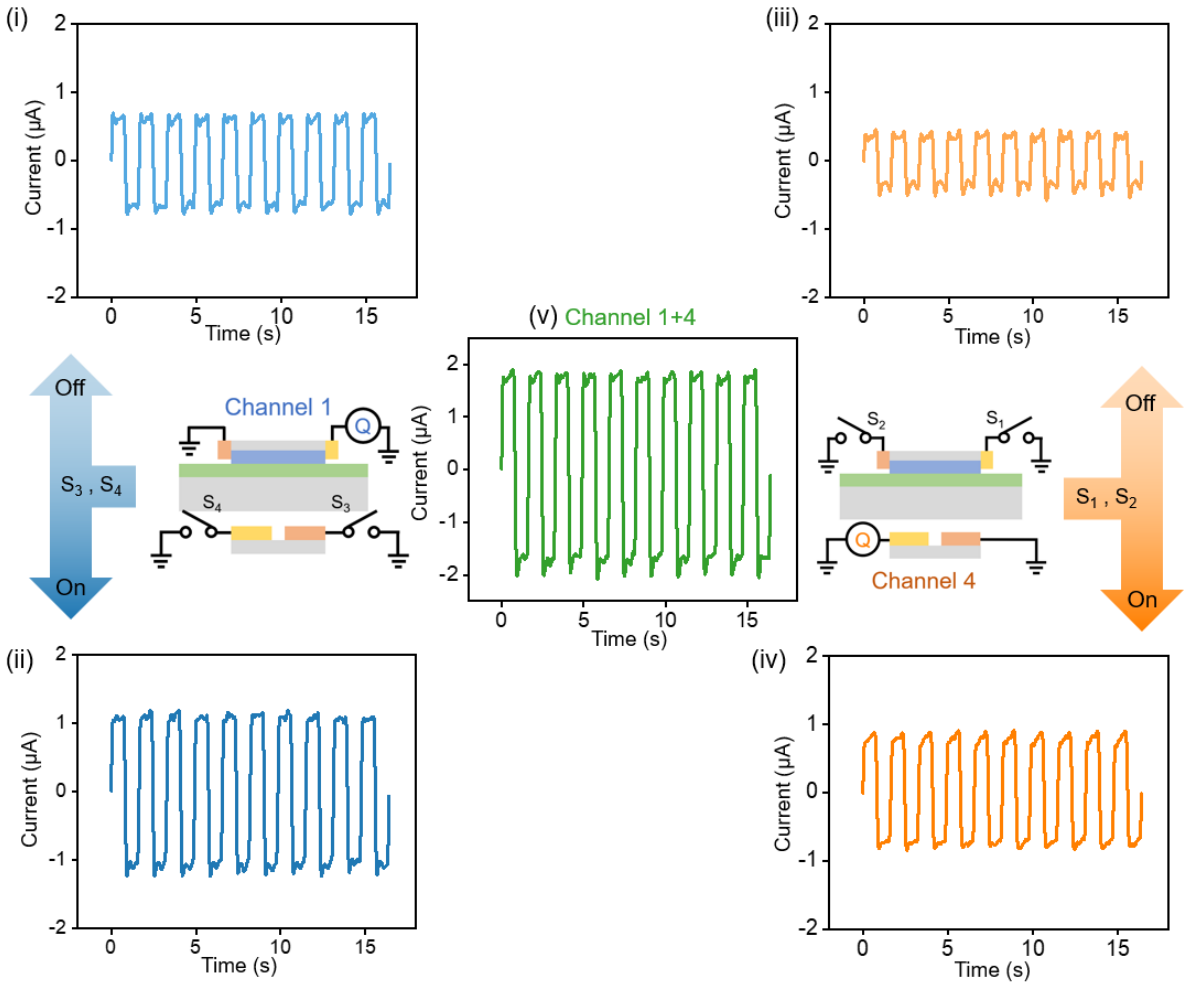

Figure S15. Output current curves of different connection modes. (i) S_3 and S_4 turn off. (ii) S_3 and S_4 turn on. (iii) S_1 and S_2 turn off. (iv) S_1 and S_2 turn on. (v) Channel 1 and Channel 4 are connected in parallel as a unified channel.

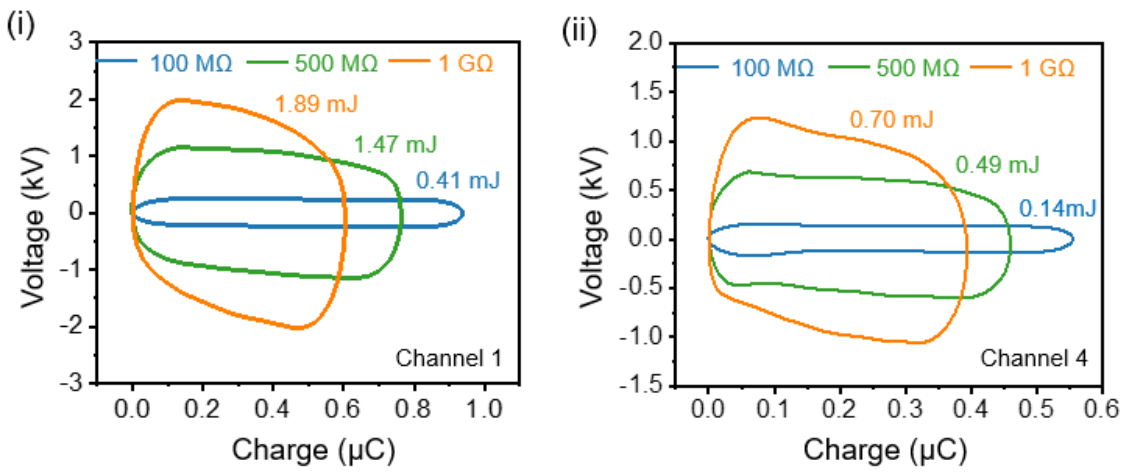

Figure S16. Voltage–charge curve under different external loads. (i) Channel 1. (ii) Channel 4.

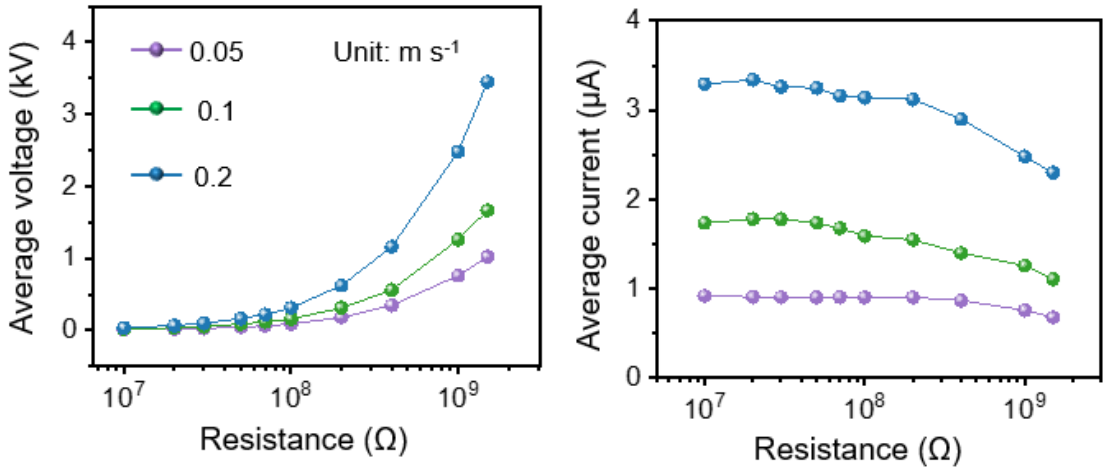

Figure S17. Average voltage and current of CTC-TENG with various external loads at different sliding speeds.

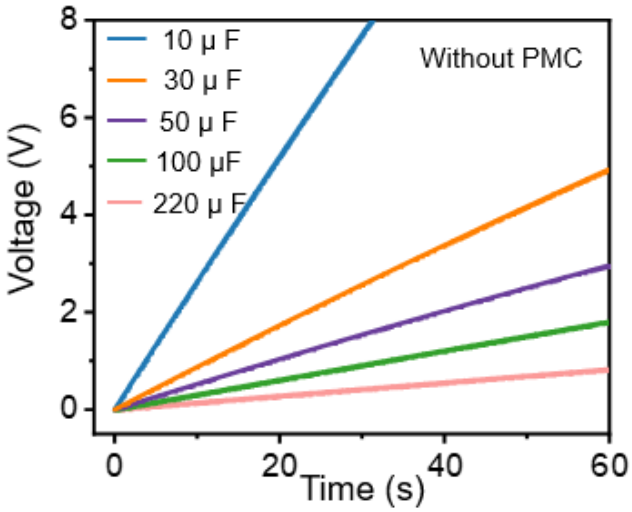

Figure S18. Voltage curves of charging capacitors by the CTC-TENG without the PMC at 0.2 m s^{-1}.

Figure S19. The construction of the visual wireless position sensing system. (i) Digital photograph of the slider. (ii) Digital photograph of the substrate. (iii) Digital photograph of the signal receiver.

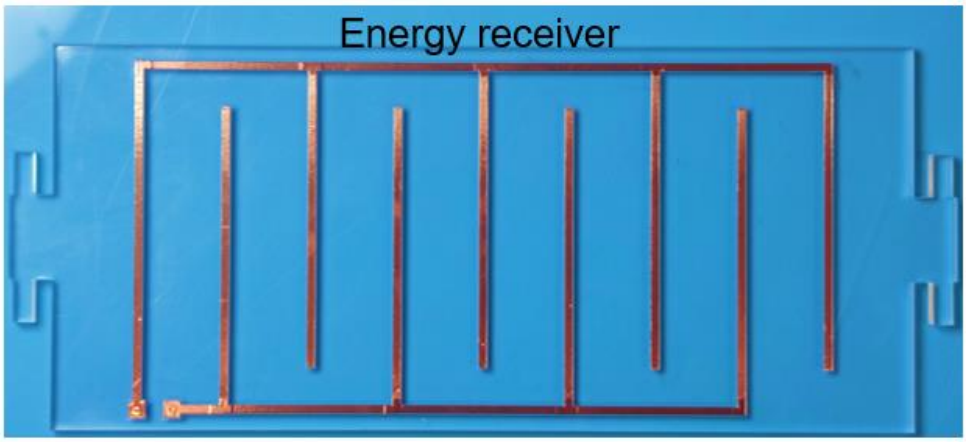

Figure S20. Digital photograph of the wireless energy receiver.

Note S1. Electric field intensity distribution between different materials in dielectric polarization enabled discharges.

To further explore the physical mechanism behind the dielectric polarization enabled discharges (DPD), we simulated the model through COMSOL software, as shown in Figure S3(i). The electric field intensity distribution curve inside the material from point A to point E is shown in Figure S3(ii). The data results show that regardless of the attenuation of the electric field during the through propagation medium, the ratio of electric field intensity between different materials is equal to the inverse ratio of their relative permittivity, which can be expressed as

$$\frac{E_1}{E_2} = \frac{\varepsilon_2}{\varepsilon_1} \quad \text{(Equation 1)}$$

where E_1/E_2, and $\varepsilon_1/\varepsilon_2$ are the electric field intensity inside the dielectric 1/2 and the relative dielectric constant of dielectric 1/2. The result is consistent with the parallel plate dielectric polarization model[1, 2]. In this process, the tribo-charge can spontaneously polarize the dielectric polymer, and build an electric field with the metal electrode, which phenomenon is called the dielectric polarization enabled discharges (DPD), the dielectric polymer is similar to a charge-transfer bridge.

Note S2. Equivalent physical model of corona discharge.

The process by which the charge collection electrode (CCE) captures the surface charge of the tribo-layer can be equivalent to a capacitive breakdown model (Figure 1c (i)), including a capacitor $C_{CCE\text{-}TL}$ (composed of CCE and tribo-layer surface), a Zener diode $D_{CCE\text{-}TL}$ (assess the threshold voltage for corona discharge), and a resistor $R_{CCE\text{-}TL}$ (equivalent resistor between CCE and tribo-layer when the corona discharge happens). Before the electrostatic breakdown occurs, $C_{CCE\text{-}TL}$ will continue to accumulate charge, and once the voltage between CCE and tribo-layer exceeds the corona discharge threshold[3], corona discharge occurs and $D_{CCE\text{-}TL}$ reverse is similar to the short circuit, with charge transfer from the tribo-layer to the CCEs for external circuit output.

Note S3. Working mechanism of the CTC-TENG on the left half of the slider.

As the negative charges on the PTFE surface move synchronously with the slider (owning to PTFE is an electret material), breaking the charge equilibrium state of the tribo-layers interface[4], as shown in Fig. 1c(i). For positive-negative charge pairs on the left half of the slider, due to the principle of electrostatic induction, the positive charges on the surface of foam induce the opposite charge on charge collection electrodes II (CCE-II), and a strong electric field is formed between CCE-II and foam[5]. Once the electric field intensity exceeds the Paschen's curve voltage value[6] (Fig. 1b(ii)), the air discharge ensues between CCE-II and foam, and the positive charges are collected flowing into the external circuit. Meanwhile, the negative charge on the PTFE surface will sustain a high potential, thereby polarizing the substrate materials. The electric dipoles are vertically and orderly arranged along the substrate, as shown in Figure S4(i). In this polarized equivalent physical model (Figure S4(ii)), the subsurface dipole of the substrate can be assumed to be the surface-bound charges, which produce the discharge effect and are collected by bottom dynamic electrodes II (BDE-II) for electrical output. Then, the upper surface dipoles of the substrate are combined with the tribo-charges. In this cycle process, CCE-II and BDE-II build a charge target transport system to collect positive-negative charge pairs of the slider's left half.

Note S4. Derive the current density of the external circuit when applying the high voltage to the electrode plates.

A constant voltage is added to the two electrodes of the dielectric polymer, and the power supply is controlled by a switch, as shown in **Fig. 2a**. It is assumed that the geometry of the system is constant, and the voltage, charge, and electric field change with time. When the switch turns on, the polarization charge density (ρ_P) of the dielectric polymer is

$$\rho_P = \frac{\partial P_r(x,t)}{\partial x} \quad \text{(Equation 2)}$$

where P_r is the polarization intensity of the dielectric polymer and x is the axis of the vertical electrode plate. The volume charge density (ρ) of the dielectric polymer is composed of polarization charge density and free charge density (ρ_r) and can be expressed as

$$\rho = \rho_r + \rho_f \quad \text{(Equation 3)}$$

according to the equation of continuity, the relationship between leakage current density (i_L) and free charge density can be expressed as

$$\frac{\partial \rho_r(x,t)}{\partial t} = -\frac{\partial i_L(x,t)}{\partial x} \quad \text{(Equation 4)}$$

the relationship between the internal electric field intensity (E) and the volume charge density of dielectric polymer can be related by the Poisson equation

$$\varepsilon_0 \varepsilon_r \frac{\partial E(x,t)}{\partial t} = \rho(x,t) \quad \text{(Equation 5)}$$

where ε_0 and ε_r are vacuum permittivity and relative permittivity of dielectric polymer. By connecting Equations (2), (3), (4), (5) and eliminating ρ_r, the total current density *I(t)* independent of space coordinates can be obtained

$$I(t) = \varepsilon_0 \varepsilon_r \frac{\partial E(x,t)}{\partial t} + \frac{\partial P_r(x,t)}{\partial t} + i_L(x,t) \quad \text{(Equation 6)}$$

if the attenuation of the polarization intensity and electric field intensity along the x direction is ignored, the total current density can be expressed as

$$I(t) = \varepsilon_0 \varepsilon_r \frac{\partial E(t)}{\partial t} + \frac{\partial P_r(t)}{\partial t} + i_L(t) \quad \text{(Equation 7)}$$

the terms on the right of Equation (7) respectively denote the induced current density, the polarization current density, and the leakage current density.

Reference

1. C. Wang, H. Guo, P. Wang, J. Li, Y. Sun and D. Zhang, *Adv. Mater.*, 2023, **35**, 2209895.
2. H. Wu, W. He, C. Shan, Z. Wang, S. Fu, Q. Tang, H. Guo, Y. Du, W. Liu and C. Hu, *Adv. Mater.*, 2022, **34**, 2109918.
3. J. Zhang, Y. Gao, D. Liu, J.-S. Zhao and J. Wang, *Nat. Commun.*, 2023, **14**, 3218.
4. C. Shan, W. He, H. Wu, S. Fu, Q. Tang, Z. Wang, Y. Du, J. Wang, H. Guo and C. Hu, *Adv. Energy Mater.*, 2022, **12**, 2200963.
5. J. Cheng, W. Ding, Y. Zi, Y. Lu, L. Ji, F. Liu, C. Wu and Z. L. Wang, *Nat. Commun.*, 2018, **9**, 3733.
6. K. Li, C. Shan, S. Fu, H. Wu, W. He, J. Wang, G. Li, Q. Mu, S. Du, Q. Zhao, C. Hu and H. Guo, *Energy Environ. Sci.*, 2024, **17**, 580-590.